Light Deflection Near Neutron Stars

U. Kraus

Abstract

This contribution describes and illustrates light deflection near neutron stars as an example of the significance of general relativity for astrophysics. First, a summary is given of the properties of photon orbits in the Schwarzschild metric, the Schwarzschild metric being a good approximation to the exterior metric of slowly rotating neutron stars. Secondly, it is illustrated how light deflection affects the observation of sources on the surface or close to the surface of a neutron star. Thirdly, it is illustrated that it is imperative to take light deflection into account when interpreting the pulse profiles of accreting X-ray pulsars, because the ratio of neutron star radius to Schwarzschild radius strongly affects the pulse profiles predicted from models of the pulsar's X-ray emission regions.

1 Introduction

When observed radiation is analyzed to deduce the properties of the source, there are three quantities of interest: photon energy, intensity and angular distribution. In order to relate the observed photon energy, intensity, and angular distribution to the photon energy, intensity, and angular distribution at the source one has to *i)* follow the photon orbit between source and observer, *ii)* find the variation of photon energy along the orbit, and *iii)* find the variation of intensity along the orbit.

This is straightforward in the absence of gravitational fields, where energy and intensity are constants along the photon orbits and photon orbits are straight lines. In the presence of gravitational fields one has to proceed in the following way:

a) Photon orbits are null geodesics $x^\mu(\lambda)$, i.e. the photon four-momentum $p^\mu(\lambda) = dx/d\lambda$ satisfies the geodesic equation and is null:

$$\frac{dp^\mu}{d\lambda} + \Gamma^\mu_{\nu\kappa}\, p^\nu p^\kappa = 0 \qquad\qquad g_{\mu\nu}p^\mu p^\nu = 0.$$

b) The energy measured by a local inertial observer with four-velocity u^μ at some location λ along the orbit is

$$E = -g_{\mu\nu}u^\mu p^\nu.$$

c) The specific intensity I_ν measured by a local inertial observer is obtained via the photon number density f which is a Lorentz invariant quantity and is constant along null geodesics in vacuum:

$$\frac{d}{d\lambda} f(x^\mu(\lambda), p^\mu(\lambda)) = 0 \qquad\qquad f = I_\nu c^2/(h^4 \nu^3).$$

2   Photons in the Schwarzschild metric

2.1   The Geodesic Equation

As a specific example for the general equations given above we will turn to photon orbits in the Schwarzschild metric.

The Schwarzschild metric is the metric in vacuum outside a spherical mass distribution. It depends on a single parameter, the Schwarzschild radius of the central mass M, defined by $r_s = 2GM/c^2$ (G the gravitational constant, c the speed of light).

In the usual Schwarzschild coordinates t, r, θ, and ϕ the Schwarzschild metric is diagonal and reads

$$g_{\mu\nu} = \text{diag}(-(1 - r_s/r), 1/(1 - r_s/r), r^2, r^2 \sin^2\theta).$$

Because of the spherical symmetry, a photon orbit is always confined to a single plane. If one chooses the polar coordinates θ and ϕ such that this plane is the equatorial plane, then $\theta = \pi/2$ is constant along the orbit and $p^\theta = d\theta/d\lambda = 0$.

The geodesic equations for the momentum components $p^t = dt/d\lambda$, $p^r = dr/d\lambda$, and $p^\phi = d\phi/d\lambda$ are:

$$\frac{dp^t}{d\lambda} + \frac{r_s}{r^2(1 - r_s/r)} p^t p^r = 0$$

$$\frac{dp^r}{d\lambda} + \frac{r_s(1 - r_s/r)}{2r^2}(p^t)^2 - \frac{r_s}{2r^2(1 - r_s/r)}(p^r)^2$$

$$- r(1 - r_s/r)(p^\phi)^2 = 0$$

$$\frac{dp^\phi}{d\lambda} + \frac{2}{r} p^\phi p^r = 0.$$

These three equations can be integrated analytically once and give

$$p^t = k^t/(1 - r_s/r) \tag{1}$$

$$p^r = \pm\sqrt{(k^t)^2 - (k^\phi)^2(1 - r_s/r)/r^2 + k^r(1 - r_s/r)} \tag{2}$$

$$p^\phi = k^\phi/r^2 \tag{3}$$

where k^t, k^r, k^ϕ are constants of integration. The constants of integration parametrize the photon orbits. The next step, therefore, is to clarify their meaning.

2.2 The Constants of Integration

The condition that p^μ be a null vector gives $0 = g_{\mu\nu}p^\mu p^\nu = k^r \quad \Rightarrow \quad k^r = 0$.

In order to see the meaning of k^t, consider a measurement of photon energy by a local inertial observer momentarily at rest. The four-velocity of such an observer is $u^\mu = (c/\sqrt{1 - r_\mathrm{s}/r}, 0, 0, 0)$ and with the expressions (1) to (3) for the photon momentum, the energy measured turns out to be $E = -g_{\mu\nu}u^\mu p^\nu = k^t c/\sqrt{1 - r_\mathrm{s}/r}$. At large r the measured energy approaches $E_\infty = k^t c$, so that the constant of integration k^t can be identified as photon energy at infinity over c.

Concerning the third constant of integration, k^ϕ, it is instructive to look at the ratio $b \equiv k^\phi/k^t$ which has the simple geometric meaning of impact parameter of the photon trajectory. This can most easily be seen in the limit of vanishing central mass $r_\mathrm{s} \to 0$ as follows. The photon orbit is completely described by three functions $t(\lambda)$, $r(\lambda)$, and $\phi(\lambda)$. If one is not interested in the lapse of coordinate time along the orbit, it is sufficient to find the trajectory $\phi(r)$, i.e., the set of all points (r, ϕ) that the photon passes through. The equation for the trajectory is

$$\frac{d\phi}{dr} = \frac{d\phi/d\lambda}{dr/d\lambda} = \frac{p^\phi}{p^r}$$

Inserting the expressions (2) and (3) for p^ϕ and p^r and setting $r_\mathrm{s} = 0$ one obtains

$$d\phi/dr = \pm b/(r^2\sqrt{1 - b^2/r^2})$$

which can be integrated to give

$$\sin(\phi - \phi_0) = \pm b/r. \tag{4}$$

Equation (4) is the equation of a straight line expressed in polar coordinates. The meaning of b is illustrated in figure 1: When a straight line is drawn parallel to the trajectory and such that it passes through the center of coordinates, then the photon trajectory is a distance b away from this straight line. Therefore, b is the impact parameter of the $(r_\mathrm{s} = 0)$-trajectory. Since the photon trajectory for nonvanishing mass $r_\mathrm{s} > 0$ approaches the zero mass trajectory at large values of r, b is also the impact parameter of the $(r_\mathrm{s} > 0)$-trajectory.
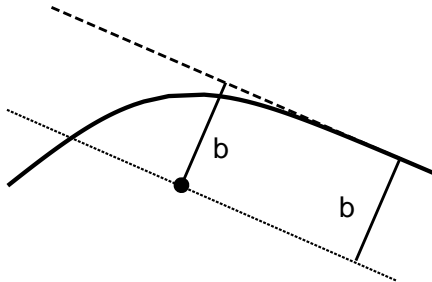
Figure 1 For $r_\mathrm{s} = 0$, the photon trajectory with impact parameter b (dashed line) is a distance b away from a parallel through the center of coordinates (dotted line). The photon trajectory for $r_\mathrm{s} > 0$ (solid line) approaches the $(r_\mathrm{s} = 0)$-trajectory for $r \gg r_\mathrm{s}$.

In summary: Photon orbits in the Schwarzschild metric are parametrized by the photon energy at infinity E_∞ and the impact parameter b. The photon four-momentum $p^\mu = dx^\mu/d\lambda$ is given by

$$p^\mu = \frac{E_\infty}{c} \left(\frac{1}{1 - r_\mathrm{s}/r}, \pm\sqrt{1 - \frac{b^2}{r^2}(1 - r_\mathrm{s}/r)}, 0, \frac{b}{r^2} \right) \tag{5}$$

and the photon trajectory $\phi(r)$ is defined by

$$\frac{d\phi}{dr} = \frac{d\phi/d\lambda}{dr/d\lambda} = \frac{p^\phi}{p^r} = \pm\frac{b}{r^2\sqrt{1 - \frac{b^2}{r^2}(1 - \frac{r_\mathrm{s}}{r})}}. \tag{6}$$

2.3   The Trajectory

The photon trajectory is given by

$$\phi(r) = \phi_0 \pm \int_{r_0}^{r} \frac{b\,dr}{r^2\sqrt{1 - \frac{b^2}{r^2}(1 - \frac{r_\mathrm{s}}{r})}}. \tag{7}$$

This integral is an elliptic integral of the first kind. There is no analytic solution, but numerical integration using standard routines is straightforward ([1]).

There are two distinct types of photon orbits, depending on whether the square root in the denominator of equation (7) has zeroes or not.

1. If $b < b_\mathrm{c} = 1.5\sqrt{3}r_\mathrm{s}$, then $\sqrt{1 - \frac{b^2}{r^2}(1 - \frac{r_\mathrm{s}}{r})} > 0$, always. These photon orbits are defined for $0 < r < \infty$. Examples are shown in figure 2: the closer b is to the critical value b_c, the stronger the deflection of the orbit from a straight line. When b gets arbitrarily close to b_c, then the orbit circles the center of coordinates arbitrarily many times. That part of the orbit where the spiralling about the center of coordinates occurs and which is nearly circular, is in the immediate vicinity of $r = 1.5r_\mathrm{s}$. The sphere with $r = 1.5r_\mathrm{s}$ is called the photon sphere.

2. If $b > b_\mathrm{c}$, then $\sqrt{1 - \frac{b^2}{r^2}(1 - \frac{r_\mathrm{s}}{r})}$ has two zeroes, r_1 and r_2, say, one inside and one outside the photon sphere: $r_1 < 1.5r_\mathrm{s} < r_2$. For each b there are two photon orbits, one defined for $0 < r < r_1$ and one defined for $r_2 < r < \infty$, i.e., photon orbits are either completely inside or completely outside the photon sphere.

   Figure 3 (left) shows photon orbits with $r > r_2$. When b approaches b_c from above, the orbit spirals more and more often around the center of coordinates. The nearly circular part of the orbit is very close to and just outside the photon sphere. Orbits with $r < r_1$ are plotted in figure 3 (right). For b approaching b_c, the orbit is very close to and just inside the photon sphere.

If the central mass is a star, then only those parts of the orbits exist that are outside the star. Since most of the deflection occurs close to $r = 1.5r_\mathrm{s}$, light deflection is important only if the radius of the star is not too large compared to its Schwarzschild radius.
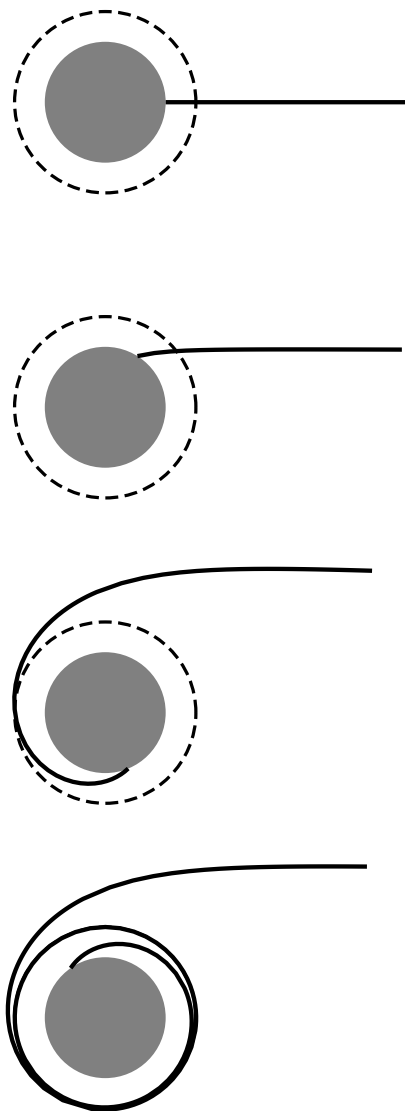
Figure 2 Photon orbits for impact parameters $b < b_{\rm c}$. The shaded area is the region $r < r_{\rm s}$, the dashed line marks the photon sphere at $r = 1.5\,r_{\rm s}$. Orbits are shown for the impact parameters 0, $0.37\,b_{\rm c}$, $0.98\,b_{\rm c}$, and $\left(1 - 2 \cdot 10^{-6}\right)b_{\rm c}$ (top to bottom).
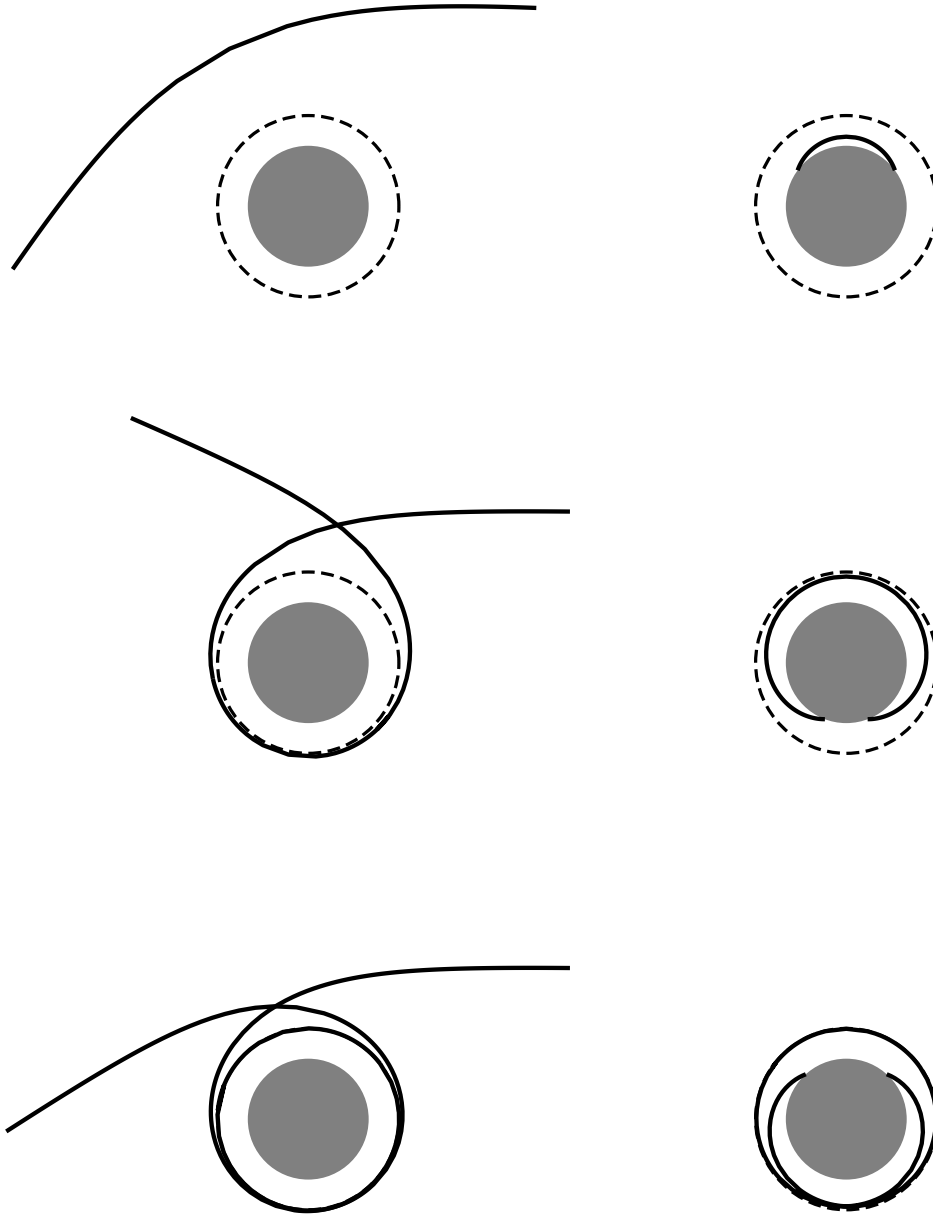
Figure 3   Photon orbits for impact parameters $b > b_c$. Orbits outside the photon sphere are shown on the left hand side for the impact parameters $1.38\,b_c$, $1.002\,b_c$, and $(1 + 1.3 \cdot 10^{-6})\,b_c$ (top to bottom). Orbits inside the photon sphere are shown on the right hand side for the impact parameters $1.23\,b_c$, $1.0043\,b_c$, and $(1 + 1.7 \cdot 10^{-5})\,b_c$ (top to bottom).

3 Light Deflection Near Neutron Stars

3.1 Masses and Radii of Neutron Stars

As we have seen, the decisive quantity regarding light deflection near a neutron star is the ratio of its radius R and its Schwarzschild radius r_s.

a) observational evidence

There are several mass determinations from the observation of neutron stars in binary systems ([2]). The most accurately known neutron star masses are those of the Hulse-Taylor binary pulsar PSR 1913+16 and its companion which are $1.442 \pm 0.003 M_\odot$ and $1.386 \pm 0.003 M_\odot$, respectively ([3]).

The less precisely determined masses of six eclipsing X-ray pulsars seem to be consistent with the "canonical" neutron star mass of $1.4 M_\odot$. Observational determinations of neutron star radii are nonexistent.

b) neutron star models

Models of nonrotating neutron stars are solutions to the Oppenheimer-Volkoff equations of hydrostatic equilibrium together with an equation of state ([2]). The key uncertainty here is the equation of state, especially at nuclear matter density and beyond. For a given equation of state the neutron star model depends on a single parameter, the central density, and there is a range of central densities which produces a series of stable neutron stars. The most massive neutron star in this series is the one with the lowest value of R/r_s. For different equations of state that are considered realistic the minimum values of R/r_s lie between 1.52 and 2.3. On the other hand one may be interested in the value of R/r_s for the $1.4 M_\odot$ neutron stars that seem to be favoured by observations. For this case, different equations of state predict values of R/r_s between 2 and 3.8. According to all of these models, a neutron star is larger than its photon sphere, but not necessarily by very much.

c) fundamental limits

Because of the uncertainty of the equation of state it is interesting to note that there are lower limits on R/r_s based only on the conditions of stability and causality ([2], [4]). According to Buchdahl's theorem, any stable star must have $R/r_s > 9/8 = 1.125$. With some additional assumptions, mainly the requirement that the speed of sound be less than the speed of light, Rhoades and Ruffini found a lower limit of $R/r_s > 1.235$. In principle, therefore, one cannot rule out the existence of ultracompact neutron stars that are smaller than their photon spheres.

3.2 Radiation from the Neutron Star Surface

Orbits of photons starting at the neutron star surface and reaching an observer some distance away are shown in figure 4. The impact parameters of these orbits lie between $b = 0$ (photon emitted radially) and some maximum value b_{max}. For a neutron star larger than its photon sphere as depicted in figure 4 the impact parameter is maximum for a photon emitted in tangential direction. From the condition that $p^r = 0$ at $r = R$ then follows with equation (5) that $b_{\mathrm{max}} = R/\sqrt{1 - r_s/R}$. For a neutron star smaller than its photon sphere, a photon that starts tangentially to the stellar surface is on an orbit
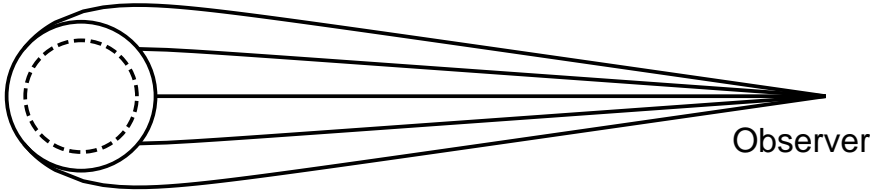
Figure 4   Orbits of photons reaching an observer from the neutron star surface. The dashed line marks the photon sphere.

confined within the photon sphere and does not reach the observer. In order for the photon to leave the photon sphere its impact parameter must be smaller than the critical impact parameter. Therefore, in this case, $b_{\max} = b_c = 1.5\sqrt{3}r_s$.

Two consequences of light deflection are immediately apparent from figure 4: enhanced surface visibility and increased angular size.

Consider an observer that is close enough to resolve the neutron star but at the same time many neutron star radii away: $r_0 \gg R$. Without light deflection the near side of the neutron star is visible, the far side hidden from view. According to figure 4, light deflection means that photons emitted on the far side may also reach the observer, so that a larger part of the surface is visible. Here are some figures that illustrate the enhanced surface visibility:

R/r_s	∞	3	2	1.75	1.509	1.5
visible part of the surface	50%	74%	94%	100%	200%	∞

For the same observer at an intermediate distance, the angular size of the star as determined by the outermost photon orbit is $\alpha = b_{\max}/r_0$ (cf. figure 5). As summarized in this table

R/r_s	∞	> 1.5	< 1.5
$b_{\max}$	R	$R/\sqrt{1 - r_s/R}$	$b_c = 1.5\sqrt{3}r_s$
$\alpha = b_{\max}/r_0$	$\alpha = \alpha(R)$	$\alpha = \alpha(M,R)$	$\alpha = \alpha(M)$

the angular size of a star larger than its photon sphere depends on both its mass and
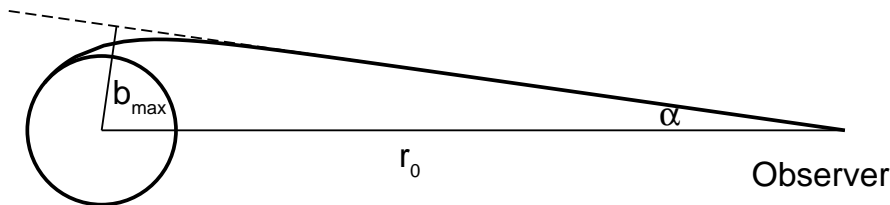
Figure 5   The angular size of the neutron star, α, is determined by the impact parameter $b_{\max}$ of the outermost photon orbit between the stellar surface and the observer.

its radius. For a star smaller than its photon sphere, the angular size is a function of mass only and completely independent of the geometric size.

Surface visibility and angular size are illustrated in figure 6 which shows five images of "neutron stars" with identical radii R and different masses so that $R/r_s = \infty$, 3, 2, 1.7 and 1.52 (after [5]). In the last case, the complete surface is visible and part of the surface is imaged a second time in a thin circular strip at the border of the image.

For a source on the neutron star surface, the photon energies measured by local inertial observers momentarily at rest at the neutron star surface and at $r \gg r_s$, respectively, are related by

$$E_\infty = E_{em} \sqrt{1 - r_s/R}$$

(cf. section 2.2). The intensity change between source and observer is then given by

$$I_\infty = I_{em}(E_\infty/E_{em})^3 = I_{em} \sqrt{1 - r_s/R}^3$$

(cf. section 1). Since the factor $\sqrt{1 - r_s/R}^3$ has the same value for all points on the neutron star, a uniformly bright star will produce a uniformly bright image.

For a given neutron star radius R, an increase in r_s makes the image both larger and fainter. These two changes compensate in the sense that the observed photon flux remains constant: The neutron star subtends a solid angle

$$\Delta\Omega = \pi\alpha^2 = \pi \frac{R^2}{r_0^2(1 - r_s/R)}.$$

The observed photon flux is then

$$N = \frac{I_\infty \Delta\Omega}{E_\infty} = \frac{I_{em}}{E_{em}} \pi \frac{R^2}{r_0^2}$$

independent of r_s.

3.3 Radiation from above the Neutron Star Surface

Since redshift and intensity change between source and observer depend on the radial coordinate of the source, the total spectrum observed from a source extended in height is a superposition of spectra with different redshifts and intensity changes.

For a source above the neutron star surface, the two major consequences of light deflection are enhanced visibility (as before) and focussing.

As regards enhanced visibility, there is a minimum height h_{min} such that a source at a height $h \geq h_{min}$ above the neutron star can never be eclipsed by the star. This is illustrated in figure 7. For an observer far away from the neutron star ($r_0 \gg R$), here are some figures for h_{min}:

R/r_s	∞	10	5	3	2.5	2	1.75
h_{min}	∞	$3.8R$	$1.32R$	$0.39R$	$0.19R$	$0.03R$	0

Neutron stars with $R/r_s \leq 1.75$ cannot eclipse anything at all!

Figure 6   Five images of "neutron stars" with identical geometrical radii R and different masses: $R/r_{\mathrm{s}} = \infty$, 3, 2, 1.7, and 1.52 (top to bottom) (after [5]). Note the enhanced surface visibility and the larger angular size with decreasing R/r_{s}.
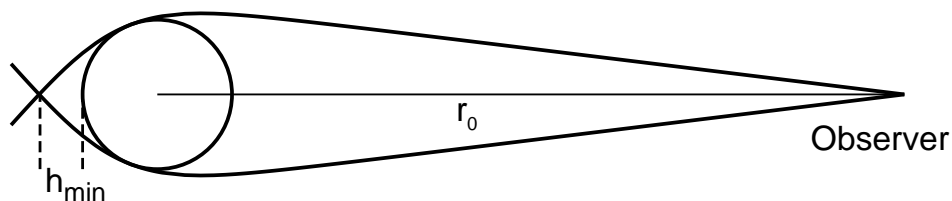
Figure 7 A source at a height $h \geq h_{\min}$ can never be eclipsed by the neutron star.

Focussing is illustrated in figure 8: A small source with isotropic emission is placed at $r = 1.25R$ (Fig. 8a). The flux measured by a distant observer with viewing angle θ is plotted in polar diagrams for $R/r_s = \infty$ (Fig. 8b) and $R/r_s = 2.5$ (Fig. 8c). In the former case, the source is visible for $\theta \leq \theta_{\max} = 126°$ (with the flux independent of θ) and hidden behind the star for $\theta > \theta_{\max}$. In the latter case, since $h = 0.025R > h_{\min} = 0.19R$, the source is always visible. At $\theta \approx 180°$ it is not only visible but also exceedingly bright!
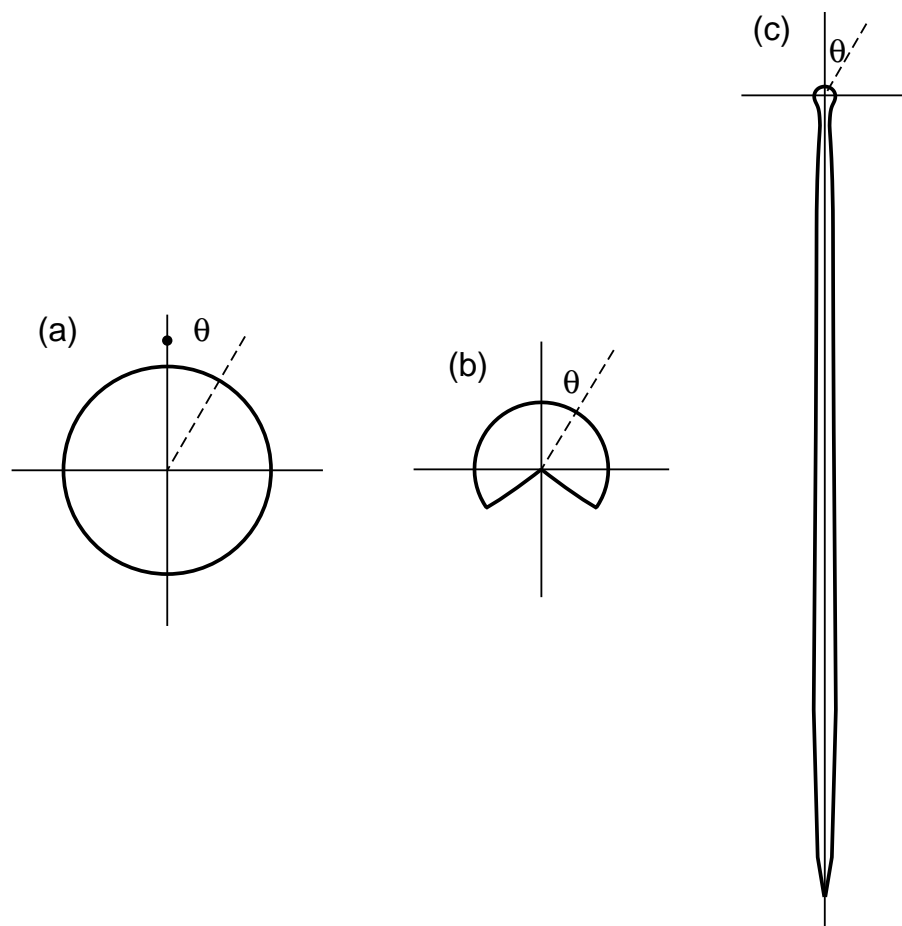
Figure 8 A small source above the neutron star (a) and the observed flux as a function of viewing direction for $R/r_s = \infty$ (b) and $R/r_s = 2.5$ (c). (Note that (b) and (c) are not to scale).
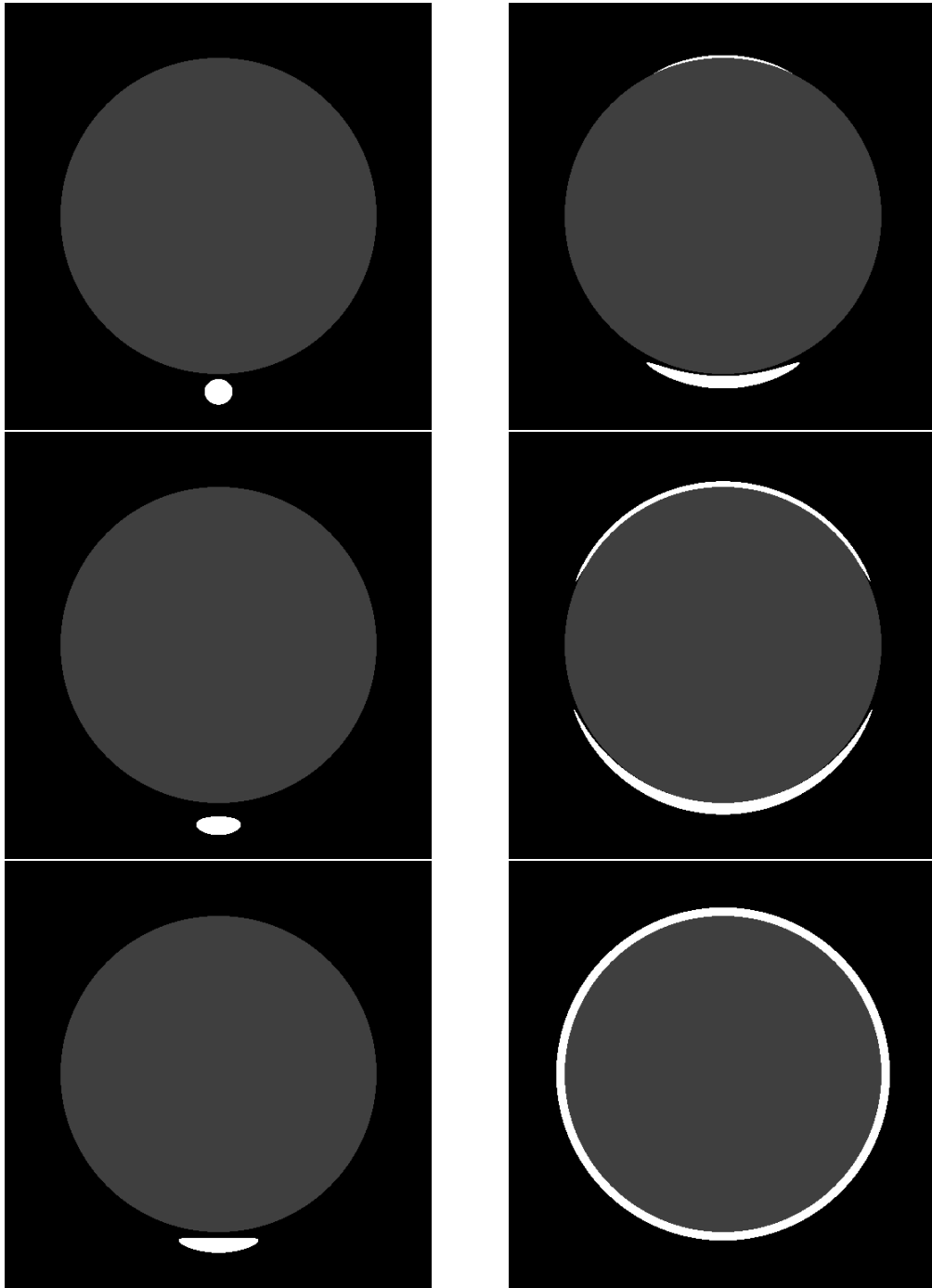
Figure 9   Visual appearance of a small source above the neutron star as seen from different directions. The viewing angle (defined to be zero when the source is in between the observer and the center of the neutron star is $90°$, $140°$, $160°$ (left, top to bottom), $170°$, $175°$, $180°$ (right, top to bottom). The images have been computed for a neutron star with $R/r_s = 2.5$ and a source that is $h = 0.25R$ above the stellar surface.

Figure 9 illustrates what the source looks like as seen from various directions θ. Note that at $\theta = 140°$ the source would be eclipsed if $R/r_s = \infty$. With $R/r_s = 2.5$ it is instead slightly elongated. At $\theta = 170°$ there are two images of the source, produced by photons passing above and below the neutron star, respectively. As θ increases, these two images grow more elongated and finally at $\theta = 180°$ merge into a ring.

4 Light Deflection in Accreting X-Ray Pulsars

An accreting X-ray pulsar is a strongly magnetized neutron star in a binary system that accretes matter from its non-degenerate companion. According to the standard model, the strong magnetic field (a typical surface field strength is $10^8\,T$) channels the matter along the magnetic field lines onto the magnetic poles where it is stopped and its kinetic energy converted to X-radiation. When the neutron star rotates, the two polar X-ray emission regions pass through the observer's field of view and therefore the X-ray flux appears pulsed with the period of rotation of the neutron star. The models of the X-ray emission region are often classified into two types:

i) polar cap models according to which the radiation is emitted from the surface of the neutron star and *ii)* column models where the site of X-ray emission is the accretion funnel just above the neutron star surface.

The significance of light deflection for the understanding of the pulse shapes of X-ray pulsars has been studied by several authors ([6], [7], [8], [9], [10], [11], [12], [13]). Here, the most simplified phenomenological models will serve as illustrative examples. A phenomenological polar cap model is shown in figure 10. There is isotropic emission from a uniformly bright circular polar cap (figure 10a). The half-opening angle α of the cap is usually estimated to be quite small; we adopt a "standard" value of $\alpha = 5°$ ([2]). The flux from this cap as measured by a distant observer depends on the viewing angle θ as shown in polar diagrams for $R/r_s = \infty$, i.e., without light deflection (figure 10b) and $R/r_s = 2.4$ (figure 10c). In the former case the flux is maximum for $\theta = 0°$ when the observer looks directly onto the polar cap and drops to zero shortly after $\theta = 90°$ when the cap disappears from view behind the neutron star. In the latter case, the flux is also maximum at $\theta = 0°$ but the cap remains visible up to $\theta = 135°$.

The changes in the angular flux distribution are much more dramatic for column
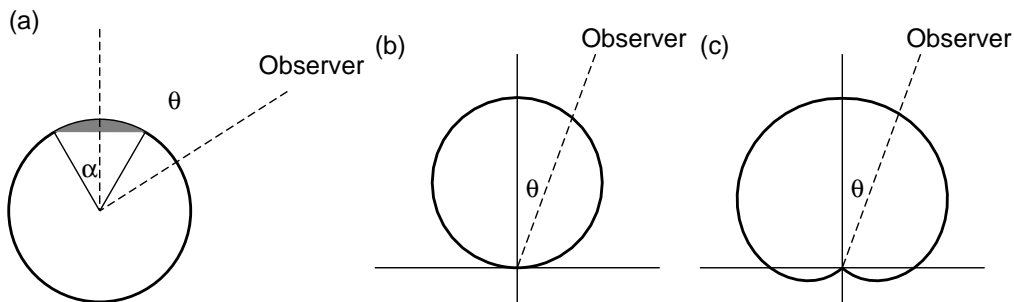
Figure 10   A phenomenological polar cap model (a) and the observed flux as a function of direction for $R/r_s = \infty$ (b) and $R/r_s = 2.4$ (c). The polar cap has a half-opening angle $\alpha = 5°$, is uniformly bright, and emits radiation isotropically. (Note that (b) and (c) are not to scale).

models as illustrated in figure 11. Here, the emission comes from the side of a truncated radial cone (figure 11a). In the simplest case, the surface of the cone is uniformly bright and emits isotropically. The dependence of observed flux on viewing angle θ for a radial cone with half-opening angle $\alpha = 5°$, truncated at $r = 1.05\,R$ is shown in polar diagrams for $R/r_{\rm s} = \infty$ (figure 11b), $R/r_{\rm s} = 2.5$ (figure 11c), and $R/r_{\rm s} = 2$ (figure 11d). Seen from above at $\theta = 0°$, the flux is zero, because the top of the truncated cone does not radiate. In figure 11b and 11c the maximum flux is seen sideways and at high θ the cone disappears behind the neutron star. In the case of figure 11d, however, the height of the cone is $h > h_{\rm min}$, so that the source is never eclipsed by the neutron star and focussing produces a sharp increase in flux towards $\theta = 180°$.

Since the pulse profiles directly reflect the angular flux distribution, it is clear that for a given model of the emission region the parameter $R/r_{\rm s}$ plays a decisive role in determining the pulse shapes. This is illustrated in figure 12 for the cap model. A neutron star with
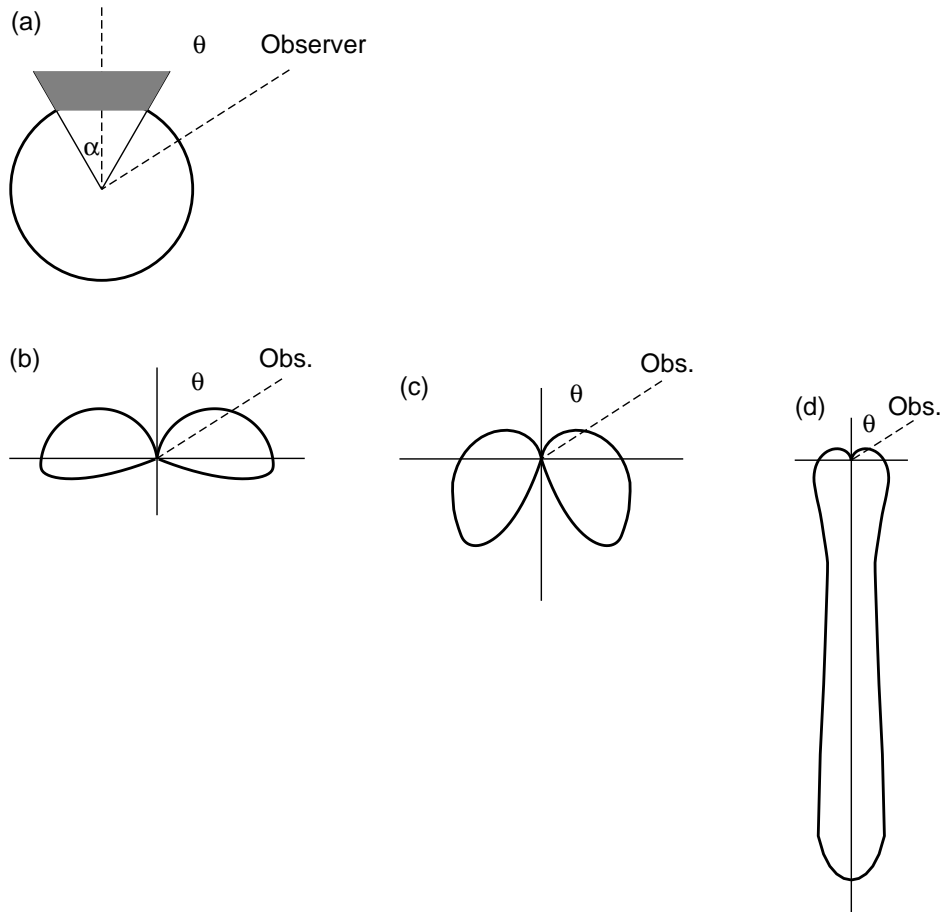
Figure 11   A phenomenological column model (a) and the observed flux as a function of direction for $R/r_{\rm s} = \infty$ (b), $R/r_{\rm s} = 2.5$ (c), and $R/r_{\rm s} = 2$ (d). The column is a truncated radial cone of half-opening angle $\alpha = 5°$ with uniform and isotropic emission from the side between radial coordinates R and $1.05\,R$. (Note that (b), (c) and (d) are not to scale).

two polar caps ($\alpha = 5°$) that are $\theta_m = 20°$ away from the rotation axis is observed at $\theta_o = 80°$ (figure 12, top). Without light deflection ($R/r_s = \infty$, Fig. 12, left) both polar caps are visible only part of the time. Their contributions to the pulse profile, labeled F_1 and F_2, therefore vanish during part of the pulse period. The total pulse profile, labeled $F_1 + F_2$, can at nearly all phases be attributed to either one or the other polar cap. At $R/r_s = 2.4$ (figure 12, right), both polar caps are always visible so that F_1 and F_2 never vanish. The total pulse profile is at all phases due to contributions of both polar caps. The most conspicuous change is the dramatic reduction in modulation of the pulse profile. This can also be understood in terms of the enhanced surface visibility: 84% of the neutron star surface are visible to the observer for $R/r_s = 2.4$. When basically everything is visible all the time, then rotation of the star cannot produce a substantial amount of modulation of the flux.

More detailed modelling of polar caps and of columns will in general predict non-uniform and non-isotropic emission. In this case, light deflection will not necessarily sup-
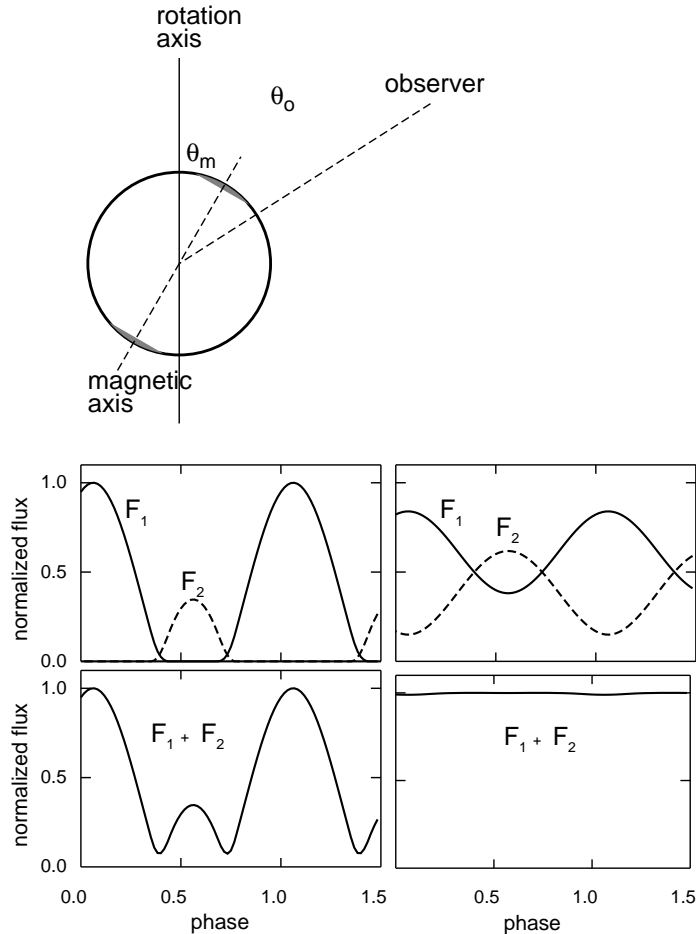
Figure 12 Pulse profiles predicted for two polar caps (top) with the same parameters as in figure 10 for $R/r_s = \infty$ (left) and $R/r_s = 2.4$ (right). The magnetic axis is $\theta_m = 20°$ away from the rotation axis and the direction of observation is $\theta_o = 80°$.

press the modulation, but it will certainly affect the predicted pulse shape in a significant way.

Bibliography

[1] Press W., Flannery B., Teukolsky S., Vetterling W. (1985): Numerical Recipes, Cambridge University Press

[2] Shapiro S., Teukolsky S. (1983): Black Holes, White Dwarfs and Neutron Stars, John Wiley & Sons

[3] Taylor J.H., and Weisberg J.M. (1989): Further experimental tests of relativistic gravity using the binary pulsar PSR 1913+16 *Ap. J.*, **345**, 434–450

[4] Weinberg S. (1972): Gravitation and Cosmology, Wiley, New York

[5] Zahn C. (1991): Vierdimensionales Ray-Tracing in einer gekrümmten Raumzeit, Diplomarbeit, Universität Stuttgart

[6] Pechenick K.R., Ftaclas C., and Cohen J.M. (1983): Hot spots on neutron stars: the near-field gravitational lens *Ap. J.*, **274**, 846–857

[7] Ftaclas C., Kearney M.W., and Pechenick K. (1986): Hot spots on neutron stars. II. The observer's sky *Ap. J.*, **300**, 203–208

[8] Riffert H., and Mészáros P. (1988): Gravitational light bending near neutron stars. I. Emission from columns and hot spots *Ap. J.*, **325**, 207–217

[9] Mészáros P., and Riffert H. (1988): Gravitational light bending near neutron stars. II. Accreting pulsar spectra as a function of phase *Ap. J.*, **327**, 712–722

[10] Nollert H.-P., Ruder H., Herold H., and Kraus U. (1989): The relativistic "looks" of a neutron star *Astron. Astrophys.*, **208**, 153–156

[11] Riffert H., Nollert H.-P., Kraus U., and Ruder H. (1993): Fitting pulse profiles of X-ray pulsars: the effects of relativistic light deflection *Ap. J.*, **406**, 195–200

[12] Bulik T., Riffert H., Mészáros P., Makishima K., Mihara T., and Thomas B. (1995): Geometry and pulse profiles of X-ray pulsars: Asymmetric relativistic fits to 4U 1538-52 and Vela X-1 *Ap. J.*, **444**, 405–414

[13] Leahy D.A., and Li L. (1995): Including the effect of gravitational light bending in X-ray profile modelling *Mon. Not. R. Astron. Soc.*, **277**, 1177-1184